Design, fabrication and characterization of a spiral phase plate

Laia Xiao Planas Toro, lplanato58@alumnes.ub.edu
Facultat de Física, Universitat de Barcelona, Diagonal 645, 08028 Barcelona, Spain.

Advisors: Jose M. Gómez Cama, jm.gomez@ub.edu
Estela Martín Badosa, estela.martinb@ub.edu

Abstract: Light beams with a helical phase front carry an orbital angular momentum which has many promising applications in several fields (microscopy, biology, astronomy, etc.). Spiral phase plates provide an efficient and cost-effective means to generate such beams. In this work, micro-scale spiral phase plates were designed and fabricated using two-photon polymerization 3D printing. The optical performance of the devices was characterized by analysing the diffraction patterns. Devices with topological charges of 1, and a number of 5 and 10 discrete phase steps were successfully manufactured and tested.
Keywords: Spiral phase plate, orbital angular momentum, vortex beam, topological charge, two-photon polymerization
SDGs: ODS 4, ODS 9

I. INTRODUCTION

Light, understood as electromagnetic fields that propagate in space, obeys the Maxwell equations, which describe it as an oscillating travelling wave. Beyond its main properties, such as intensity, frequency or polarization, light also carries angular momentum which can be decomposed into the spin angular momentum (SAM) and the orbital angular momentum (OAM).

SAM, first introduced by Poynting *et al.* [1] for circularly polarized light, is associated with the polarization state of the wave. In contrast, OAM arises from the spatial structure of the wavefront, specifically phase distributions with azimuthal dependency as described in 1992 by Allen *et al.* [2]. Surprisingly, even in the single-photon limit this behaviour can be observed [3].

The discovery of such a property has enabled many applications in different fields, among these are microscopy, biology, astronomy, and quantum communications [4]. For example, in imaging and super-resolution microscopy, OAM beams help surpass the diffraction limit (e.g., STED microscopy [5]). Considering the fact that individual photons can carry an OAM opens up a wide range of possibilities in the quantum communication field, as compared to SAM, which can only assume two possible states. OAM can assume an infinite number of discrete integer values, making it a powerful resource for high-dimensional encoding [6, 7].

Beams carrying OAM are characterized by the presence of an isolated central intensity zero. In the paraxial regime, they can be described as Laguerre-Gaussian modes characterized by two parameters ℓ and p. The topological charge ℓ corresponds to the strength of the central singularity and indicates the number of twists of the helical wavefront. The index p refers to the number of radial nodes.

To generate OAM beams from conventional Gaussian beams, several methods have been proposed, including spatial light modulators, q-plates, and diffractive optical elements [2, 8]. In this work, we focus on the Spiral Phase Plate (SPP), a passive optical component that imparts a helical phase shift by means of a thickness gradient increasing azimuthally. First demonstrated by Beijersbergen *et al.* [9], the SPP produces an optical vortex beam with phase $\exp(i\ell\theta)$, where ℓ is the topological charge. This phase delay is physically realized via a twisted, staircase-like optical surface centered around the beam axis. The resulting beam will possess the topological charge imposed by the SPP but will inherit the p from the incident wavefront (Gaussian beam $p = 0$).

In this work, we present the design, two-photon polymerization (2PP) fabrication, and optical characterization of a miniaturized SPP through diffraction pattern analysis, demonstrating its ability to generate high-purity optical vortex beams.

II. MATERIALS AND METHODS

A. Design

SPP is implemented as a transparent optical element with an increasing thickness profile. The total optical path difference introduced by the SPP is given by:

$$OPD = \frac{2\pi}{\lambda} \cdot \Delta n \cdot h(\theta) \tag{1}$$

where Δn is the refractive index contrast between the material and the surrounding medium, λ is the operating wavelength, and $h(\theta)$ is the azimuthal thickness function. To generate the desired helical phase, the height profile must satisfy:

$$h(\theta) = \frac{\ell\lambda}{2\pi\Delta n} \cdot \theta, \quad \theta \in [0, 2\pi) \tag{2}$$

Due to the fabrication constraints, the SPP design was discretized into N steps; thus, each sector, which has a

constant thickness, introduces a uniform phase shift of $2\pi/N$.

The device was designed for operation at $\lambda = 632.8$ nm with a topological charge $\ell = 1$ and $N = 5, 10$ phase levels. The outer radius of the SPP was set to $r = 100$ μm, due to the printing area. The height variation across 2π was calculated to be $h_{\max} = \ell\lambda/\Delta n \approx 1.22$ μm, considering the refractive index difference of $\Delta n = 0.516$.

In total, six different devices, all with a radius of 100 μm were designed, whose features are shown in Table I.

Device	ℓ	N	h (μm)	h_b (μm)	Δ_h (μm)	$\Delta\phi$ (rad)
L15a	1	5	2.226	1	0.2452	1.257
L15b	1	5	3.226	2	0.2452	1.257
L15c	1	5	11.226	10	0.2452	1.257
L110a	1	10	2.226	1	0.1226	0.628
L110b	1	10	3.226	2	0.1226	0.628
L110c	1	10	11.226	10	0.1226	0.628

TABLE I: Devices designed, topological charge, number of steps, total height, base height, and height/phase change per step.

In addition, two variations of the *l15a* and *l110a* devices were designed with a surrounding linear grating covering an area of 1 mm^2. The grating, featuring a π phase shift with a periodicity of 700 nm and a height of 0.6 μm, was implemented to deflect light away from the area of interest.

The 3D models of the SPPs were generated using an OpenSCAD script and exported in STL format. This model served as the input for the fabrication process.

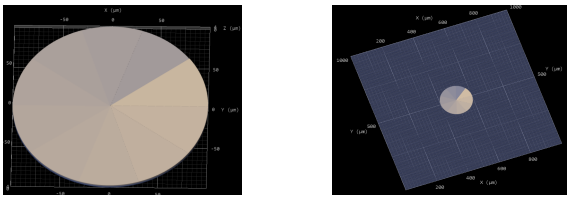

(a) (b)

FIG. 1: Schematic of the STL designs for (a) L110b and (b) L110g.

B. Fabrication process

The micro SPPs were fabricated using two-photon polymerization (2PP), a 3D printing high-resolution direct laser writing technique capable of producing complex microstructures via a nonlinear absorption of ultrashort femtosecond laser pulses to induce localized polymerization within a photosensitive material.

In our case, a commercial Nanoscribe Photonic Professional GT2 system was used, which enabled a resolution of 100 nm. It is equipped with a femtosecond pulsed laser (780 nm, 80 MHz repetition rate, <100 fs pulse duration). Due to the galvo diameter, the effective printing field is 200 μm, which implies that, for larger structures, the overall object must be split into separate pieces, each printed sequentially. The photoresist used was IP-L (Nanoscribe) using a 63X objective (NA = 1.4) in oil immersion configuration, printing on a 0.3 mm borosilicate substrate.

The STL design was processed with the system slicing software (Describe) to generate the laser scanning path. The fabrication parameters were optimized to ensure mechanical stability and for optimal results: slicing distance 0.1 μm, hatching distance 0.2 μm, laser power of 50% for solid parts and of 100% for contouring. Fabricated SPP designs required between 5' - 25' and 1 hour if printed with the grating. Only SPPs that do not require splitting were considered (except for the grating).

After exposure, the sample was developed by immersing it in SU8-Developer for 9' and then rinsed in isopropanol. Post-processing included drying the sample with a nitrogen gun and inspecting the fabricated structure using an optical microscope first and then using a confocal optical profiler (Sensofar).

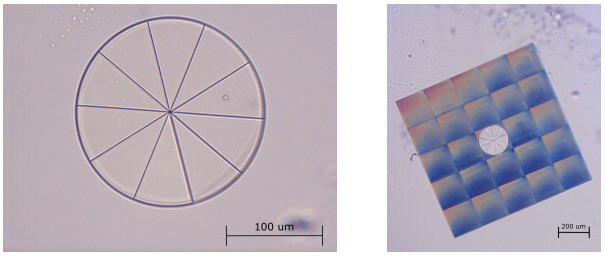

(a) (b)

FIG. 2: Optical microscope images of devices (a) L110b (b) L110g.

C. Simulation

Before the optical characterisation of the vortex beams generated using the manufactured devices, to further understand the optics behind, simulations of the far-field and propagation intensity distributions were computed in a Python environment using the fast Fourier transform (FFT) (Fig. 3). To avoid mathematical artefacts and aliasing, a large number of pixels was used.

D. Experimental set-up and intensity measurement

For the optical characterization, the optical setup displayed in Fig. 8 was built using a Gaussian beam emitted by a HeNe laser ($\lambda = 632.8$ nm, beam-waist $w_0 \approx 3$ mm). Since the devices fabricated have a size of 200 μm, the

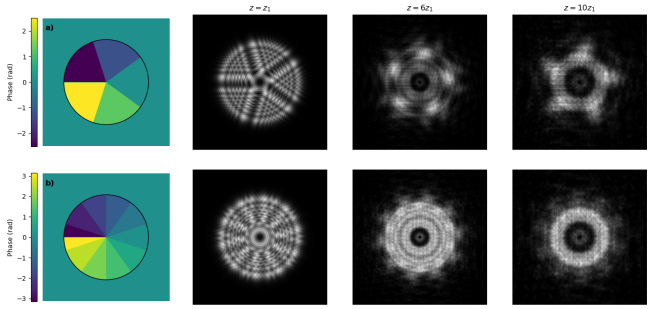

FIG. 3: Simulated propagation of the SPP phase pattern considering Fresnel diffraction for (a) L15 and (b) L110 .

incident light beam had to be adjusted by means of a telescope system composed of a lens (L1) of $f_1 = 500\ mm$ and a 20x objective (NA = 0.5, $f_{obj} = 8\ mm$) (OBJ), giving a 60-times reduction of the beam, that is $w_0' \approx 50\ \mu m$. Before the sample (SPP), a pinhole (P) was placed to act as a spatial filter to block higher frequency components (noise, distortion, speckle, etc.). Then the sample was mounted on an XYZ manual linear stage for micrometric positioning. This step was crucial to guarantee a flat-centered wavefront illumination of the SPP to obtain a correct far-field pattern; additionally, the beam after the pinhole presented a high divergence (short Rayleigh distance); therefore, the sample had to be placed as close as possible to the pinhole.

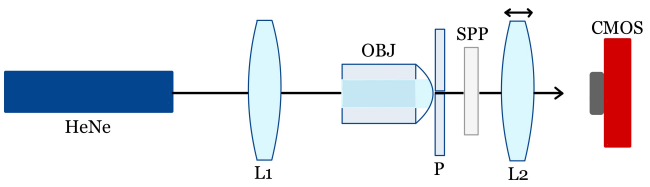

FIG. 4: Optical setup for the generation of Laguerre-Gaussian beams.

Finally, an imaging system was implemented using a lens (L_2) ($f_2 = 25\ mm$) and a CMOS camera (Thorlabs, CS165MU Zelux) both mounted on a cage system. By adjusting the position of the lens, pictures on the image plane and the far-field plane were acquired. The intensity patterns obtained were analysed using the software ImageJ. First, a centre of mass was manually found to perform a radially-averaged intensity profile. Then, to ensure a proper comparison between them, each profile was normalised.

III. RESULTS AND DISCUSSION

A. Manufactured device

From all the samples fabricated, it could be concluded that the height of the SPPs played a key role in the results obtained, as the designed samples with the lowest height presented folding and adhesion problems to the substrate, in contrast to those with additional base layers. Alternatively, when the samples were printed in contact with other structures (grating or other SPPs), they did not present folding defects. To further ensure the SPPs stability, for each printed layer, a contouring exposure with higher laser power compared to the solid part was performed. By doing so, the external parts of the elements presented a more uniform and smooth appearance. Other

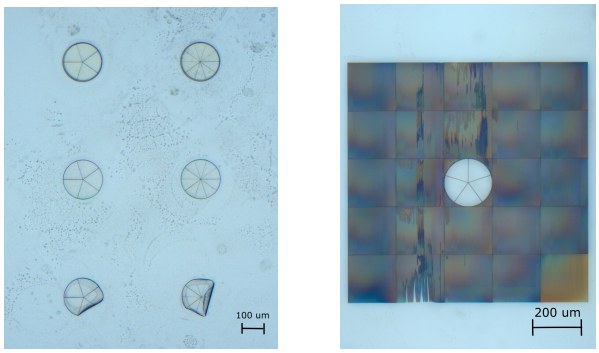

(a) (b)

FIG. 5: Optical microscope images of (a) from top to bottom L15c/L110c, L15b/L110b, L15a/L110a (b) L15g.

challenges faced during fabrication included printing the grating, as it required splitting, and to avoid degradation, recalibration to find the interface of the substrate in each step was needed. Despite this, as the structure included thin lines of less than a micrometer of height/width, for several samples the grating presented defects, as Fig. 5 shows in addition to evidence of splitting and stitching. To reduce all the defects, the development time was reduced for all designs from the original 20-minute recipe to 9'. Although the printed structures' quality improved, it also resulted in a higher presence of resist residues in the substrate. If the development is reduced below 9', sub-development effects (stuck lines, less smoothness) arise. Adhesion problems can also be due to the substrate not being properly cleaned or presenting surface irregularities. Pretreating the substrate with a plasma treatment was used in some cases to improve adhesion, but it did not change the result in any significant way.

Regarding vertical resolution, the limit of steps that was accomplished for $\ell = 1$ SPPs was $N = 10$. Higher number of steps implied $\Delta h < 100\ nm$, which is below the Nanoscribe resolution. To inspect the printed step heights, the data from the optical profiler was analyzed.

Fig. 6 shows that the limit of resolution can be achieved; however, the overall height does not exactly correspond to the designed one for all the steps.

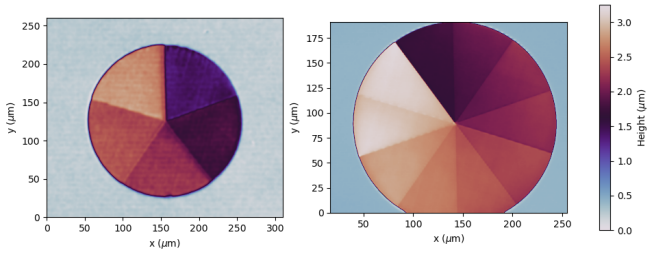

FIG. 6: Topological images obtained using the confocal optical profiler for L15 and L110.

Profile measurements are very susceptible to vibrations, which added to the fabrication/development alterations in the process, may have affected the results. It must be remarked that the profile test was only performed on samples that were not used in the optical setup afterwards, in order to preserve them; therefore, to determine the real discrepancy between fabrication and design, further measurements are needed.

B. Optical characterization

Six different devices were analysed using the optical setup described in the previous section, which were divided into the number of steps and in terms of having or not having a grating around them.

When simulating the far-field intensity distributions of $\ell = 1$, the homogeneity in intensity of the resulting beam depended greatly on the number of steps of the SPP: the higher the number of steps, the smoother the pattern obtained. This result reproduces the simulated intensity distribution as seen in Fig. 7, although it is more in accordance with Fresnel propagation (Fig. 3, right). The experimental measurements of the intensity distribution for L15b and L110b were in accordance with the simulated behaviour as the latter shows a uniform 'doughnut' shape, whereas the former presents five spikes (each corresponding to a phase shift).

Following a more qualitative comparison studying the effect of the number of steps, a quantitative comparison of the effect of the surrounding grating was performed. When comparing the experimental images of the far-field intensity, it is seen that the devices with gratings present a brighter 'doughnut' shape around the centre. Both samples with grating, though still present inhomogeneities around the center. The step quantization is evident in L15g, while in L10g, there's a section with less intensity than the rest that could be due to some fabrication defect. From simulations, not fully closed rings are usually due to a misalignment of the sample and the light beam or small deviations of the total phase shift.

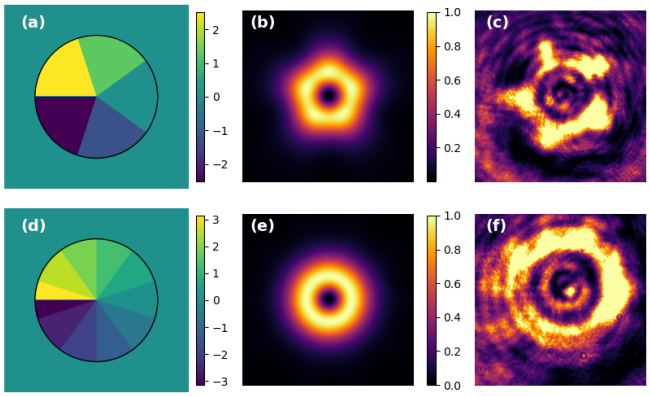

FIG. 7: Simulated phase pattern, simulated and experimental intensity distribution in a far-field plane of Gaussian beams after SPP corresponding to L15b and L110b.

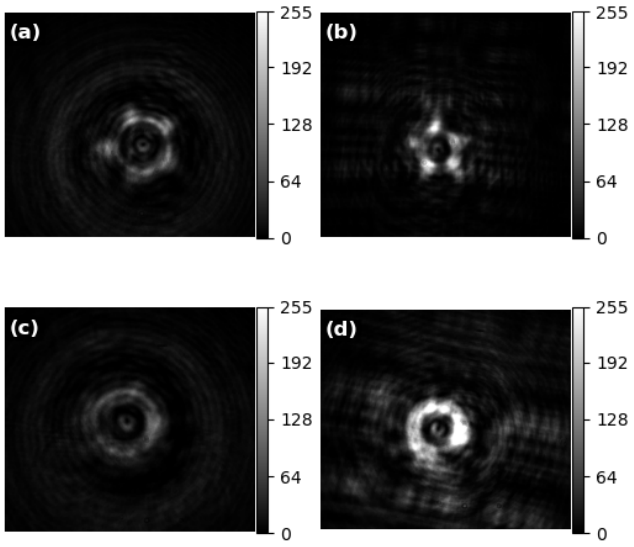

FIG. 8: Experimental intensity distributions images obtained with the CMOS camera of SPPs (a)L15c (b) L15g (c) L110c (d) L110g.

When analysing the azimuthally averaged intensity profiles (Fig. 9), the profiles were shifted to correct the fact that the images were not taken in the exact same plane. It should be noted that having different base heights results in a change of the image/Fourier plane positions. Despite this, it can be seen that the inner intensity peak of the sample with grating is less than the one without it, and the main ring is brighter. To confirm the advantage of using a grating around the device, further tests should be carried out, trying to ensure that the images were taken under the same experimental conditions. Theoretically, the intensity profiles for beams with a topological charge of $\ell = 1$ should present a single intensity peak corresponding to the intensity ring. However, in all the

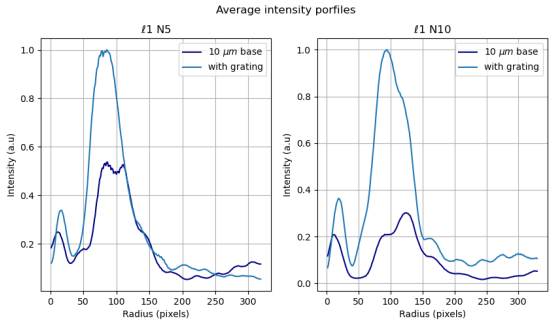

FIG. 9: Azimuthal averaged intensity profiles for L15c/L15g and L110c/L110g.

images acquired, several rings are present surrounding the centre. These additional rings may indicate that the profiles do not correspond to the Fourier plane but to Fresnel diffraction near the Fourier plane of the SPP as simulated cases suggest (Fig. 3).

IV. CONCLUSION

In conclusion, using 2PP 3D printing, micro-scale spiral phase plates have been fabricated and characterized, demonstrating the significant influence of structural and process parameters on the performance of the final devices.

From the fabrication perspective, the height and substrate adhesion emerged as determining factors; the taller structures or those in contact with larger structures, such as the grating, being more stable. To improve the feature definitions, the reduction of the development time was adopted as a strategy, although trade-offs such as residual resist and incomplete development were observed.

Regarding the optical characterization part, the number of quantization steps in the SPPs had a clear impact on the intensity profiles measured: the higher the number of steps, the more homogeneous the intensity profiles were obtained. The effect of adding a grating appeared to enhance the main ring and reduce the central intensity. Despite this, some fabrication defects and alignment inconsistencies could have affected performance. Images obtained aligned more closely with Fresnel propagation when compared with simulations. This suggests that the experimental observation plane has an offset from the true Fourier plane. Differences in height between designed and printed devices, as well as different measurement conditions, made it difficult to confirm all simulation predictions quantitatively. Additionally, the profile analysis was only performed on separate test samples.

Future work will include improving, on one hand, the height accuracy fabrication by exploring other fabrication recipes, and on the other hand, achieving a more consistent and controlled optical measurement. Exploring alternative optical elements compatible with 2PP, such as other diffractive structures or holograms, may further enhance beam quality.

Acknowledgments

I would like to thank my supervisors Estela Martín Badosa and Jose M. Gómez Cama for their guidance and support. Besides, I would like to thank the members of the QComms UB group, especially Lidia Lozano. Additionally, Nick Toledo and Jaume Caus for their help in the lab. Lastly, I would like to express my gratitude to my friends Marc, Victor, Pol and my parents. This study was supported by IECC, MCIN with funding from European Union NextGenerationEU(PRTR-C17.I1) and by Generalitat de Catalunya. We acknowledge funding from Grant PID2023-147475NB-I0 by MCIN/AEI/10.13039/5011 00011033 and Grants 2021SGR01095, and 2021SGR01108 by Generalitat de Catalunya. This project has received funding from the European Union's Digital Europe Programme under grant agreement no. 101084035.

[1] J. H. Poynting, Proceedings of The Royal Society A: Mathematical, Physical and Engineering Sciences (1909).
[2] L. Allen, M. W. Beijersbergen, R. Spreeuw, and J. Woerdman, Physical review A **45**, 8185 (1992).
[3] J. P. Torres and L. Torner, *Twisted photons: applications of light with orbital angular momentum* (John Wiley & Sons, 2011).
[4] Y. Lian, X. Qi, Y. Wang, Z. Bai, Y. Wang, and Z. Lu, Optics and Lasers in Engineering **151**, 106923 (2022).
[5] K. I. Willig, S. O. Rizzoli, V. Westphal, R. Jahn, and S. W. Hell, Nature **440**, 935–939 (2006).
[6] J. Wang, J. Liu, S. Li, Y. Zhao, J. Du, and L. Zhu, Nanophotonics **11**, 645 (2022).
[7] A. Mair, A. Vaziri, G. Weihs, and A. Zeilinger, Nature **412**, 313 (2001).
[8] L. Marrucci, C. Manzo, and D. Paparo, Physical review letters **96**, 163905 (2006).
[9] M. Beijersbergen, R. Coerwinkel, M. Kristensen, and J. Woerdman, Optics communications **112**, 321 (1994).

Disseny, fabricació i caracterització d'una placa de fase espiral

Laia Xiao Planas Toro, lplanato58@alumnes.ub.edu
Facultat de Física, Universitat de Barcelona, Diagonal 645, 08028 Barcelona, Spain.

Advisors: Jose M. Gómez Cama, jm.gomez@ub.edu
Estela Martín Badosa, estela.martinb@ub.edu

Resum: Els feixos de llum amb un front de fase helicoïdal transporten moment angular orbital que és una propietat amb moltes aplicacions en diferents àmbits (microscopia, biologia, astronomia, etc.). Una manera eficient i econòmica de produir feixos de llum amb tals característiques és utilitzar plaques de fase espiral. En aquest treball, s'han dissenyat i fabricat plaques de fase espiral a escala micromètrica mitjançant impressió 3D per polimerització de dos fotons. El rendiment òptic dels dispositius s'ha caracteritzat a partir de l'anàlisi de patrons de difracció. S'han fabricat i examinat amb èxit dispositius amb càrrega topològica 1 i amb 5 i 10 nivells de quantificació de fase respectivament.
Paraules clau: Placa de fase espiral, moment angular orbital, feix vòrtex, càrrega topològica, polimerització de dos fotons.
ODSs: Aquest TFG està relacionat amb els Objectius de Desenvolupament Sostenible (SDGs) 4 i 9.

Objectius de Desenvolupament Sostenible (ODSs o SDGs)

1. Fi de la es desigualtats		10. Reducció de les desigualtats	
2. Fam zero		11. Ciutats i comunitats sostenibles	
3. Salut i benestar		12. Consum i producció responsables	
4. Educació de qualitat	X	13. Acció climàtica	
5. Igualtat de gènere		14. Vida submarina	
6. Aigua neta i sanejament		15. Vida terrestre	
7. Energia neta i sostenible		16. Pau, justícia i institucions sòlides	
8. Treball digne i creixement econòmic		17. Aliança pels objectius	
9. Indústria, innovació, infraestructures	X		

El contingut d'aquest TFG s'ha desenvolupat en un entorn educatiu, que contribueix a l'educació a nivell universitari (ODS 4). Per altra banda, les tècniques utilitzades són tecnologies emergents que poden tenir un impacte en la indústria i promoure la innovació en el disseny i la fabricació d'elements òptics (ODS 9).

GRAPHICAL ABSTRACT